NUMERICAL SIMULATION OF FLOW CONTROL BY SYNTHETIC JET ACTUATION

Jasper M. Tomas , Edwin T.A. van der Weide , Hein de Vries , Harry W.M. Hoeijmakers
Group Engineering Fluid Dynamics, University of Twente
P.O. Box 217, 7500 AE Enschede, The Netherlands

Keywords: *Aerodynamics (High Lift, Flow Control, Computational Fluid Dynamics, Synthetic Jet)*

Abstract

Numerical simulations of active flow control have been carried out for the flow around the NACA0018 profile for Mach = 0.15, $Re = 2 \times 10^6$, $\alpha = 15^o$ using the Unsteady Reynolds Averaged Navier-Stokes (URANS) equations. Two types of flow control, zero-net-mass jets (synthetic jets) and continuously blowing jets, have been considered to delay the onset of separation. The synthetic jets have been applied to the 2D situation, i.e. infinitely long slits in the spanwise, for which the angle between the jet and surface normal has been varied to study the effect on the separation. For the continuously blowing jets the effect of 3D mixing is taken into account and an optimization of several jet parameters has been carried out to obtain the best result possible.

1 Introduction

During the take-off and landing phases of an aircraft slats and flaps are employed to increase the lift of the wing. Often flow separation is present for these high lift conditions, which can decrease the performance of the wing significantly. This is an undesirable situation since larger flaps are needed to deliver the required amount of lift and consequently the weight and hence fuel consumption of the aircraft will increase.

In the framework of the Smart Fixed Wing Aircraft work package of the EU Clean Sky program it is investigated whether or not flow control, both active and passive, is capable to increase the effectiveness of flaps by reducing the region in which the flow is separated. Boundary layer separation is accompanied with low momentum in the near wall region of the airfoil. Separation control focuses on the addition of momentum to the boundary layer such that it can handle the adverse pressure gradient typically occurring on the aft part of the airfoil. Adding momentum to the boundary layer can be accomplished as follows:

A Interchange low momentum flow from the boundary layer with high momentum flow from the free stream by removal of the low momentum boundary layer fluid by suction.

B Tangential injection of high momentum fluid.

C Creation of large vortical structures to create a transfer of momentum from the high momentum free stream to the low momentum boundary layer and vice versa (also known as mixing), see figure 2.

In terms of blowing or suction, Method A can be achieved by suction only, while Method B and C are achieved by blowing only. Hence it can be expected that a combination of suction and blowing, such as synthetic jets, might be an efficient mechanism for separation control.

In the Smart Fixed Wing Aircraft work package experimental data is available for the DLR F15 wing geometry, see Fig 1, which is there-

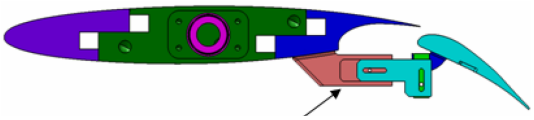

Fig. 1 The DLR F15 geometry. Figure taken from [1]

fore the geometry of choice for numerically simulating flow control. However, this geometry is still relatively complicated and therefore an even simpler geometry has been chosen in this initial study. It turns out that the character of the separation on the flap of the DLR-F15 is very similar to the trailing edge separation occurring on the NACA0018 airfoil at high angle of attack. Therefore flow control on this NACA airfoil will be investigated in the present study. In section 2 a synthetic jet will be simulated assuming an infinitely long slit in the spanwise direction. Therefore the flow can be assumed to be 2D, which leads to a reduction of the computational requirements. Two different cases are considered, namely injection normal to the surface, i.e. 90 degree pitch angle, and injection with a pitch angle of 25 degrees.

The assumption of a 2D flow field prohibits the creation of streamwise vorticity, which is known to be an effective mixing mechanism, see figure 2. Method C is not used when infinitely long slits are employed and therefore in section 3, slits with a finite length are used, leading to a 3D flow field. Still assuming an infinite span wing and no variation in the slit geometry, periodic boundary conditions can be applied in the spanwise direction, leading to a finite computational domain that contains only one slit. In the present study it is attempted to obtain the optimal slit configuration by applying an optimization algorithm. However, the required computational resources were not available to carry out this optimization for the case with synthetic jets, which requires a time accurate simulation. Therefore continuously blowing jets are used instead for which it may be assumed that the flow is steady.

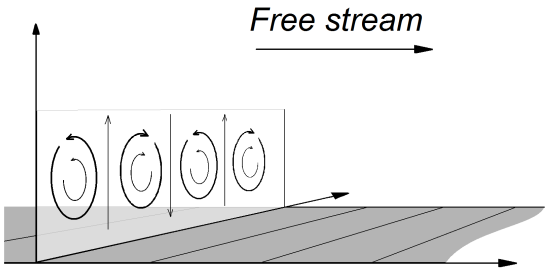

Fig. 2 Concept of mixing of boundary layer with free stream; vortices are shown in the plane perpendicular to the free stream direction

In section 4 conclusions are drawn and some recommendations for future work are given.

All simulations presented in this work have been carried out using the SUmb multiblock structured compressible flow solver [2]. SUmb uses a second-order accurate cell-centered finite volume formulation. For all the cases presented here the inviscid terms are discretized using Roe's approximate Riemann solver in combination with a linear reconstruction in terms of the primitive variables, i.e. no limiter is used, while the viscous terms are discretized by means of a central difference stencil.

2 2D Synthetic jets

In this section three types of synthetic jet actuation are investigated for the NACA0018 profile. The free-stream conditions used are Mach = 0.15, Reynolds = $2 \cdot 10^6$ and $\alpha = 15°$. The Mach and Reynolds number are identical to those used for the DLR-F15 configuration [1], while the angle of attack is chosen such that a significant separation region occurs at the trailing edge, see Fig. 3.

2.1 The mass and momentum coefficients

If we consider an arbitrary two-dimensional airfoil with a continuously blowing jet at the surface of the airfoil, the momentum added by the jet to the flow per unit span is:

$$J = \int_{L_o} \rho_o (\vec{u}_o \cdot \vec{n}_o)^2 \, dl \qquad (1)$$

where L_o is the chordwise width of the orifice, ρ_o is the density at the orifice, $\vec{u}_o$ is the velocity vec-

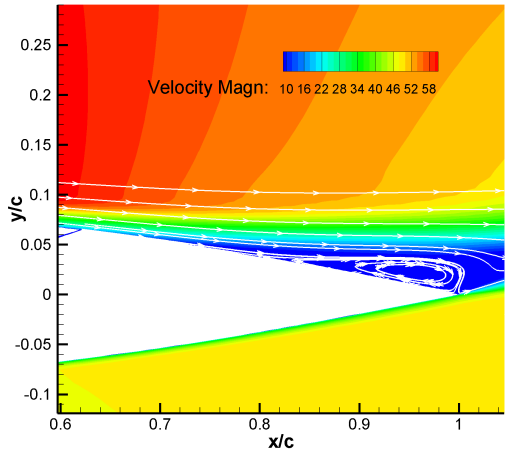

Fig. 3 Velocity magnitude in m/s and streamlines for the NACA0018 baseline configuration without control. Mach = 0.15, Re = $2 \cdot 10^6$ and $\alpha = 15°$

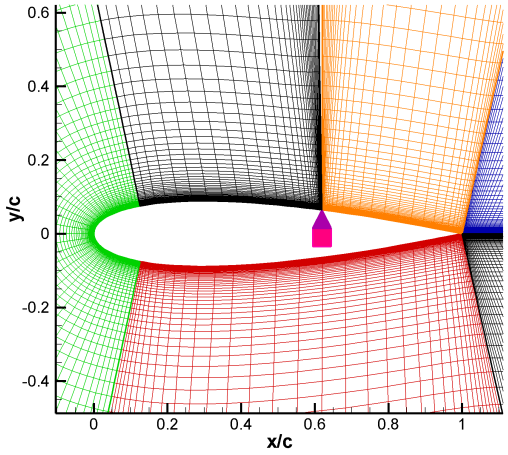

Fig. 4 Zoom of the computational grid including a synthetic jet actuator for the NACA0018

tor at the orifice surface and $\vec{n}_o$ is the unit vector normal to the orifice area pointing in the direction of the flow field. In general the momentum added to the flow is given as the momentum coefficient C_μ; the ratio of the momentum added to the flow and the dynamic pressure of the free stream multiplied by chord length:

$$C_\mu = \frac{J}{qc} = \frac{J}{\frac{1}{2}\rho_\infty (U_\infty)^2 c} \tag{2}$$

where J is the momentum in the jet, equation (1), q is the free stream dynamic pressure, c is the chord of the airfoil, and ρ_∞ and U_∞ are the free stream density and velocity magnitude, respectively. Here the airfoil chord is used as reference length.

A similar derivation can be carried out for the mass addition to the flow at the orifice. The mass coefficient reads:

$$M_j = \frac{\dot{m}_o}{\rho_\infty U_\infty c} \tag{3}$$

where $\dot{m}_o$ is the mass flow added to the flow, given by:

$$\dot{m}_o = \int_{L_o} \rho_o \vec{u}_o \cdot \vec{n}_o \, dl \tag{4}$$

Accordingly, when oscillatory blowing and suction is applied, we can define an oscillatory momentum coefficient:

$$c_\mu = \frac{j^{\text{rms}}}{qc} = \frac{j^{\text{rms}}}{\frac{1}{2}\rho_\infty (U_\infty)^2 c} \tag{5}$$

where j^{rms} is defined as:

$$j^{\text{rms}} = \int_{L_o} \left(\rho_o (\vec{u}_o \cdot \vec{n}_o)^2\right)^{\text{rms}} dl \tag{6}$$

where the superscript 'rms' indicates that the root mean square of the quantity is taken. In the remainder of this paper these coefficients will be used to quantify the mass and momentum addition to the flow by means of the (synthetic) jet.

2.2 Computational setup

In order to simulate the effect of the synthetic jets for the baseline configuration described above, these control devices are added to the computational domain, see Fig. 4. This is achieved by modeling a chamber inside the airfoil with a harmonically vibrating wall, i.e. a piston. The cham-

Conf.	Pitch angle α_j	Stroke/ chord	Remarks
SJ1	90°	$0.8 \cdot 10^{-2}$	sharp inlet
SJ2	90°	$1.6 \cdot 10^{-2}$	smooth inlet
SJ3	25°	$1.6 \cdot 10^{-2}$	smooth inlet

Table 1 Details of three synthetic jets considered

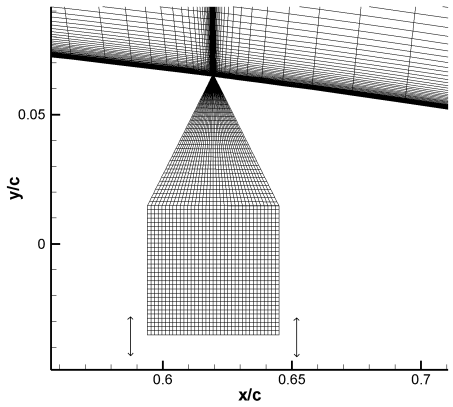

Fig. 5 Grid for actuator SJ1.

ber is connected to the outside by a small orifice through which the fluid is blown and sucked. Three different synthetic jet actuators are considered, whose geometries are described in table 1 and shown in Figs. 5 to 7. In these figures the arrows indicate the direction of the piston motion. The main differences between these configurations are the shape of the converging part to the orifice and the pitch angle α_j, which is defined as the angle between the orifice duct and the airfoil surface. The actuators displace the same amount of fluid at the piston wall, although actuator SJ1 has a smaller stroke and therefore a larger piston width, see table 1. All three actuator orifices are located at $x/c = 0.62$. This is $0.13c$ upstream of the location where separation occurs in the baseline configuration. This position is chosen because actuation should take place near the point of separation, but not downstream of this location. The width of the actuator orifice, L_o, is chosen such that the influence of the actuator to the flow should be minimized when it is not active. According to [3] the diameter of the actuator's orifice should not be larger than 5%-20% of the boundary layer thickness. In this case, the boundary layer thickness is around $2 \cdot 10^{-2}c$ at the location considered. Therefore, for all present investigations the orifice width, L_o, measures $10^{-3}c$.

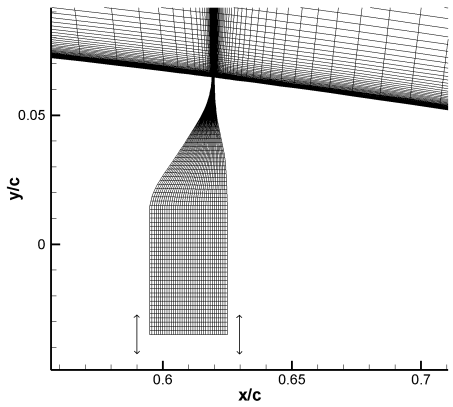

Fig. 6 Grid for actuator SJ2.

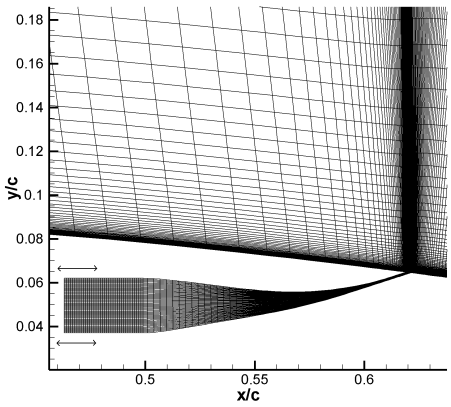

Fig. 7 Grid for actuator SJ3.

Of the three mechanisms of adding momentum to the boundary layer, configurations SJ1 and SJ2 use method A, i.e. suction of the low momentum fluid. Configuration SJ3 also uses method B, tangential injection, but, as mentioned above, none of these configurations uses method C, mixing by means of large vortical structures.

The frequency of actuation, f_e, is chosen according to the observation that the most efficient momentum addition takes place when the reduced forcing frequency, F^+, equals unity [4]. This reduced forcing frequency F^+ is defined as:

$$F^+ = \frac{f_e X_{TE}}{U_\infty} \tag{7}$$

Here X_{TE} is the distance of the actuator orifice from the trailing edge of the airfoil and U_∞ the free stream velocity.

For the three cases considered the frequency of actuation f_e is 134 Hz. It was found that time steps of $T/100$ gave a periodic converged solution for all three cases, with T the time needed for one actuation cycle, which equals:

$$T = \frac{1}{f_e} \tag{8}$$

2.3 Results

The flow is assumed to be fully turbulent with the turbulent quantities modeled using the Spalart-Allmaras turbulence model [5]. The governing equations, i.e. URANS and the transport equation of the Spalart-Allmaras model, $\frac{dU}{dt}+R(U)=0$, are integrated in time until the periodic state is reached. The time integration scheme used is the second-order implicit backward difference formula, i.e.

$$\frac{dU}{dt}=\frac{3U^{n+1}-4U^{n}+U^{n-1}}{2\Delta t}, \tag{9}$$

where the time index $n+1$ indicates the new state. Combined with the spatial discretization for $R(U)$, this results in the following set of algebraic equations for the new state $n+1$

$$\frac{3(VU)^{n+1}-4(VU)^{n}+(VU)^{n-1}}{2\Delta t}+R(U^{n+1})=0. \tag{10}$$

Here V is the volume of each computational cell and U the set of conserved variables at the cell centers. Due to the motion of the piston this volume can be different for each time index, which is taken into account in equation (10). Equation (10) is solved using the dual time stepping technique [6], where well-known convergence acceleration techniques are employed, such as multigrid and local time stepping.

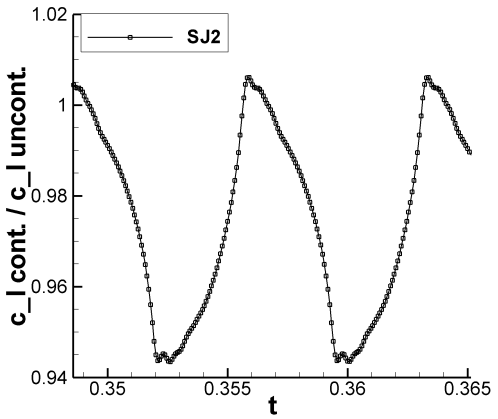

Fig. 9 NACA0018 at $\alpha=15^{\circ}$ and $\mathrm{Re}=2\cdot10^{6}$. Periodically varying c_l for SJ2. Plotted is the ratio of the c_l for the controlled case and the c_l of the uncontrolled case.

Fig. 8 to 10 show the converged periodic lift coefficients, relative to the uncontrolled case, for the three actuators considered. It is clear that for the cases SJ1 and SJ2 the synthetic jet actuation leads to the average lift coefficient being even lower than that for the uncontrolled case. Table 2 summarizes the results for lift and drag and also lists the momentum coefficients c_μ. For case SJ3, however, a significant increase in the lift is observed, on average about 10%, while the drag is reduced by almost 20%. This behavior can be explained by considering the average flow field for these cases, see Figs. 11 to 13. When these figures are compared to Fig. 3 for the uncontrolled

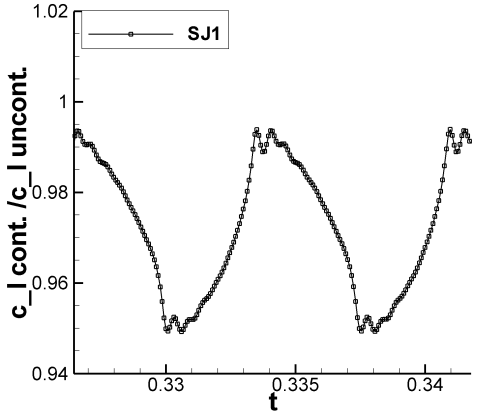

Fig. 8 NACA0018 at $\alpha=15^{\circ}$ and $\mathrm{Re}=2\cdot10^{6}$. Periodically varying c_l for SJ1. Plotted is the ratio of the c_l for the controlled case and the c_l of the uncontrolled case.

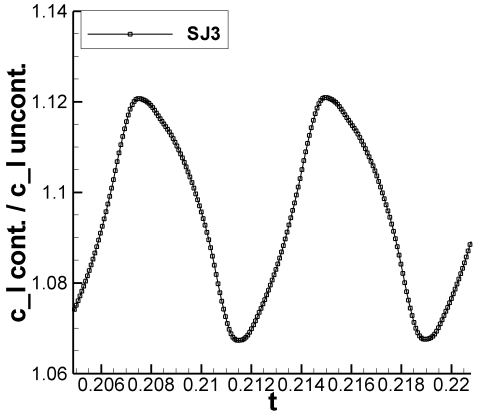

Fig. 10 NACA0018 at $\alpha=15^{\circ}$ and $\mathrm{Re}=2\cdot10^{6}$. Periodically varying c_l for SJ3. Plotted is the ratio of the c_l for the controlled case and the c_l of the uncontrolled case.

Case	c_μ in %	$\bar{c_l}/c_{l_u}$	$\bar{c_d}/c_{d_u}$
SJ1	0.27	0.972	1.099
SJ2	0.71	0.973	1.195
SJ3	0.58	1.097	0.811

Table 2 NACA0018 at $\alpha = 15^\circ$ and $Re = 2 \cdot 10^6$. Summary of the results for the synthetic jet actuation

case, it is clear that for the cases with injection perpendicular to the surface, SJ1 and SJ2, the separation region hardly changes. However, for the case with almost tangential injection, SJ3, the separation has completely disappeared, leading to a higher lift and lower drag.

From this study it can therefore be concluded that for 2D synthetic jets injection perpendicular to the surface is not a good option for separation control. During the suction part of the cycle low momentum fluid is removed, but this effect is completely neutralized during the blowing part of the cycle and the resulting net effect is slightly negative. On the other hand, tangential injection, SJ3, does lead to a positive effect since the separation completely disappears for the case considered. However, the momentum coefficient c_μ chosen to obtain a positive effect is rather high, table 2, and might not be realizable in practice.

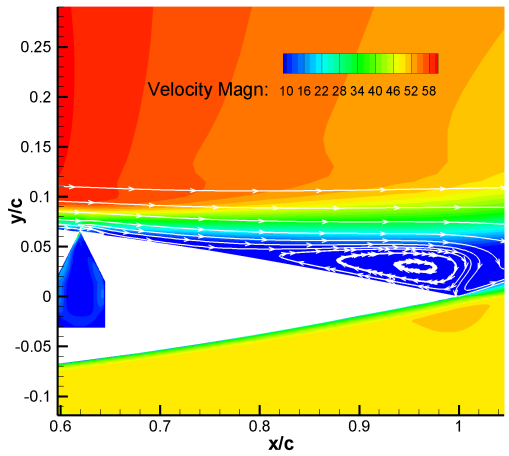

Fig. 11 NACA0018 at $\alpha = 15^\circ$ and $Re = 2 \cdot 10^6$. Average velocity magnitude in m/s and streamlines for SJ1.

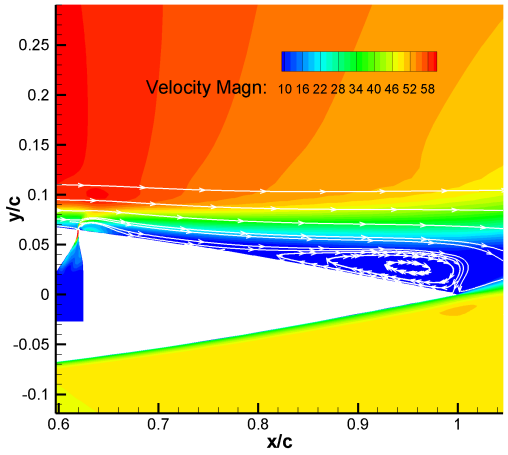

Fig. 12 NACA0018 at $\alpha = 15^\circ$ and $Re = 2 \cdot 10^6$. Average velocity magnitude in m/s and streamlines for SJ2.

3 Optimization of a continuously blowing jet

The results in the preceding section show that for the 2D situation for synthetic jets a positive effect is only obtained when momentum is injected tangentially, i.e. method B. However, it is known that this method only gives positive results when the velocity of the jet has a magnitude comparable to that of the velocity of the free stream [7]. In the case of an aircraft in landing or take-off configuration the velocity of the free stream can be well over 50 m/s, which is a velocity out of reach of currently available practical synthetic jet

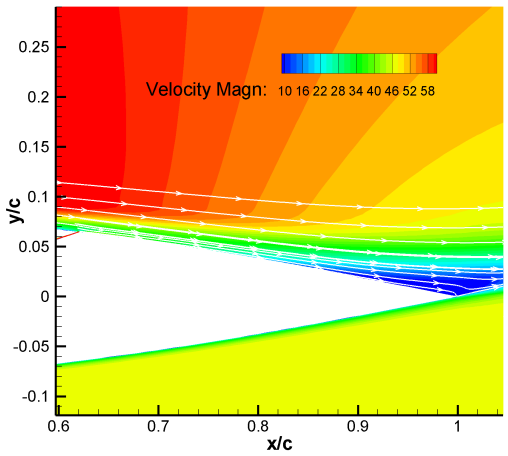

Fig. 13 NACA0018 at $\alpha = 15^\circ$ and $Re = 2 \cdot 10^6$. Average velocity magnitude in m/s and streamlines for SJ3.

actuators. This brings up the question whether such an actuator can be applied for the remaining Method C, the effect of mixing, to add momentum to the boundary layer during the blowing phase of the synthetic jet.

As the effect of mixing is primarily a 3D flow phenomenon a fully 3D unsteady flow simulation should be carried out if synthetic jets are employed. Unfortunately the available computational resources are inadequate to perform a series of such simulations. Therefore three-dimensional continuously blowing jets are considered instead, because these devices allow for a steady flow analysis. However, it is far from clear what the optimal geometry and jet velocity should be to effectively delay flow separation. If the distance between the jets is too small the situation will be similar to the 2D case for which no mixing occurs. On the other hand, when the distance between the jets is too large the effect of flow control is negligible. Hence an optimum will exist somewhere in between these two extremes. Finding this optimum by trial and error is very time consuming, also because multiple design variables should be considered for the jet (e.g. chordwise slot width, spanwise slot length, distance between slots), see section 3.1.

Fortunately, this problem is well-suited for a gradient-based optimization technique, which allows the efficient computation of the optimum in an automated manner.

3.1 Description of the optimization problem

The first task in an optimization problem is the choice of the design parameters. In this case the following parameters have been considered, see also Figs. 14 and 15.

- $L_o^* = L_o/\cos(\alpha_j)$: Slot length in the plane of the airfoil surface.
- W_o: Slot width.
- W_s: Section width: $W_s = D_s + W_o$, where D_s is the distance between the slots.
- α_j: Jet pitch angle.

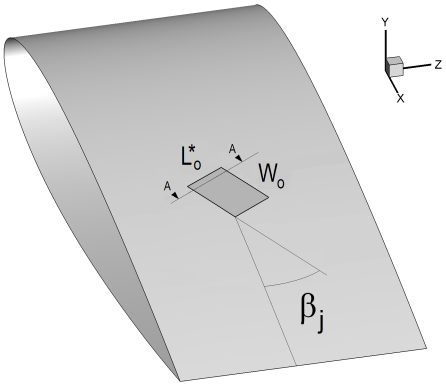

Fig. 14 Definition of the design variables for the optimization.

- β_j: Jet skew angle.

Although the chordwise location of the slot is also a design parameter, it was chosen not to consider this as a design parameter, because it led to problems with the automatic grid generation algorithm. Additional computations have indicated that the results are not very sensitive to this location as long as the slot is located between 40 and 70 percent chord. Another design variable would be the jet velocity. However, in this initial study this parameter is kept constant at 60 m/s, which corresponds to 1.2 U_∞. Furthermore, the section width W_s is chosen such that the slot area per unit span is equal for all cases. This is an attempt to keep the added mass and momentum per unit span the same. Hence, 4 independent design

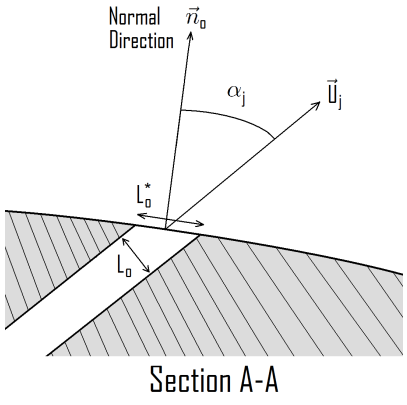

Fig. 15 Section A-A of figure 14.

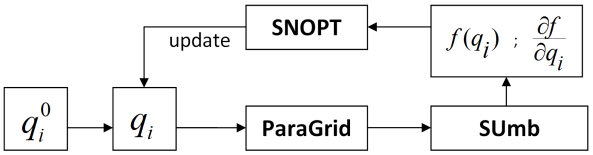

Fig. 16 Optimization procedure; q_i is set of design parameters.

variables remain, L_o, W_o, α_j and β_j.

Fig. 16 shows a schematic of the optimization procedure. Here q_i is the set of design parameters, q_i^0 the corresponding initial guess, ParaGrid is an automatic grid generation algorithm tailored for this application and SUmb is the flow solver. SNOPT (Sparse Nonlinear) OPTimizer) is a software package that uses a gradient-based method to solve constrained optimization problems, which can be linear or nonlinear [8]. Finally $f(q_i)$ is the objective function to be optimized. For this case the objective function is the lift coefficient, which should be maximized by SNOPT, because maximum lift is reached for a either fully attached flow or just a mildly separated flow.

SNOPT uses the gradients of the objective function to determine the search direction. In each iteration the design variables given by SNOPT define a new configuration that is evaluated in SUmb. This gives the value (lift coefficient) of the objective function for this set of design variables. In addition, the algorithm requires the gradients of the objective function. The gradients are approximated by finite differencing. One-sided differences are used in order to minimize the number of evaluations required.

$$\frac{\partial f}{\partial q_n} = \frac{f(q_i + \delta_{in}\Delta q_i) - f(q_i)}{\delta_{in}\Delta q_i},\ i = 1,\cdots,4 \quad (11)$$

where subscript n indicates each design variable, and δ_{in} is the Kronecker delta.

3.2 Results

SNOPT is a gradient based optimizer, hence it will converge to a local optimum. It is not known whether this optimum is the global optimum or not. Therefore, the initial set of design variables is of influence on the result; if the initial guess is close to a local optimum, SNOPT will converge to that solution. Therefore the optimization process has been applied twice, which will be referred to as Run 1 and Run 2, respectively. The initial design variables for both runs are listed in table 3.

Parameter		Run 1	Run 2
Slot length	L_o	0.006 m	0.006 m
Sloth width	W_o	0.020 m	0.020 m
Jet pitch angle	α_j	30°	5°
Jet skew angle	β_j	45°	5°

Table 3 Initial design variables for optimization Run 1 and optimization Run 2

Run 1 converged in 46 iterations while Run 2 took only 24 iterations to converge. The results are listed in Table 4. The lift coefficient found in Run 2 is higher than the one found in Run 1. Apparently Run 1 converged to a local maximum, while Run 2 appears to have converged to the global maximum (although this cannot be guaranteed). In this optimal geometry both α_j and β_j are zero, leading to a jet normal to the surface. This is in contrast to the case using the 2D synthetic jet, where normal injection is not the optimal configuration.

The geometry found in Run 2 is shown in Figure 17. Three adjacent sections are shown. The corresponding flow field is shown in Figs. 18 and 19. Especially from Fig. 19 it is clear that two counterrotating chordwise vortices are present in

Parameter		Run 1	Run 2
Slot length	L_o	0.02102 m	0.00525 m
Sloth width	W_o	0.01082 m	0.02010 m
Jet pitch angle	α_j	28.338°	0°
Jet skew angle	β_j	53.6196°	0°
Lift coefficient	c_l/c_{l_u}	1.09135	1.1945

Table 4 Results for optimization Run 1 and optimization Run 2. c_{l_u} is the lift coefficient of the uncontrolled case.

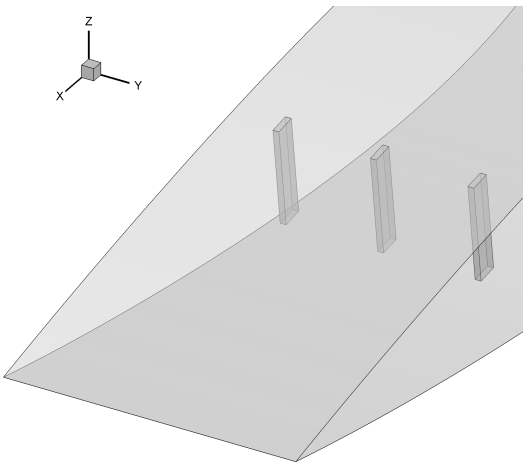

Fig. 17 NACA0018 at $\alpha = 15°$ and $Re = 2 \cdot 10^6$. Optimal geometry found in Run 2; three adjacent airfoil sections are shown; the design parameters are listed in Table 4.

the flow field. These vortices are created by the continuously blowing jet, which therefore acts as a vortex generator. As can be seen from Fig. 18 the vortices are still present outside the boundary layer and hence mixing of high momentum fluid is guaranteed.

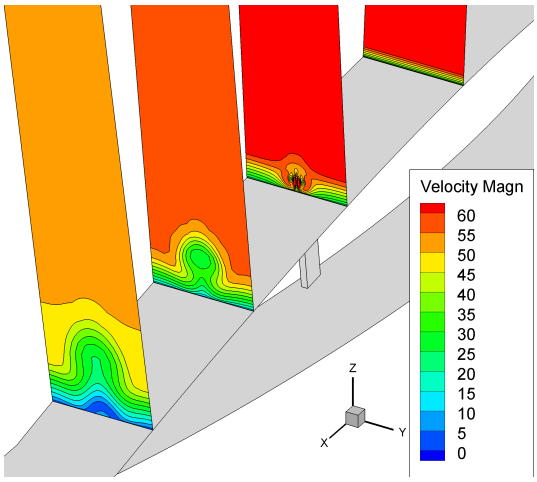

Fig. 18 NACA0018 at $\alpha = 15°$ and $Re = 2 \cdot 10^6$. Contours of velocity magnitude, $|\vec{u}|$, in m/s in planes normal to the airfoil surface at several chordwise positions for the optimal geometry of Run 2, see Table 4.

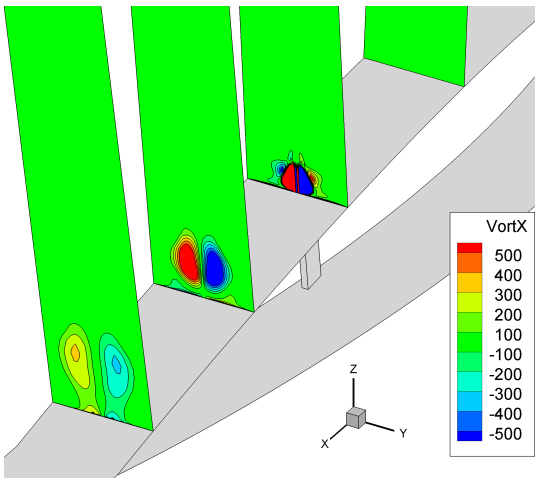

Fig. 19 NACA0018 at $\alpha = 15°$ and $Re = 2 \cdot 10^6$. Contours of chordwise vorticity component, ω_x, in s^{-1} in planes normal to the airfoil surface at several chordwise positions for the optimal geometry of Run 2, see Table 4.

4 Conclusions and Recommendations

In this study two types of active flow control to delay the onset of separation have been considered for the NACA0018 airfoil for the flow conditions Mach = 0.15, $Re = 2 \times 10^6$, $\alpha = 15^o$. The types considered are synthetic jets using an infinitely long slit in the spanwise direction, allowing a 2D analysis, and an infinite periodic spanwise series of continuously blowing jets, allowing periodic boundary conditions in spanwise direction. The simulations with the synthetic jet show that injection normal to the surface has a detrimental effect on the flow separation, i.e. the average lift coefficient decreases while the drag increases. Apparently the positive effect of removing low momentum fluid, Method A, during the suction phase of the cycle, is completely neutralized during the blowing phase. On the other hand (almost) tangential injection of high momentum fluid almost eliminates the separation for this case and leads to an increase in lift of almost 10%, while the drag is reduced by almost 20%. Unfortunately, this increase in performance is realized using a rather high value of the momentum coefficient c_μ, namely 0.58%, which is most likely too high for currently available (and practi-

cally usable) devices. Reducing c_μ to more realistic values led to results that did not improve the flow significantly over that of the baseline configuration, because the jet velocity is too low. This is in agreement with what is found in [7].

For the continuously blowing jets the effect of mixing due to the generation of large chordwise vortical structures, Method C, is the main mechanism to replace low momentum fluid in the boundary layer by high momentum fluid. The result of the optimization shows that, when chosen carefully, a row of jets can indeed reduce or even completely remove the flow separation region. An interesting detail is that the optimal configuration is such that the injection is normal to the surface, this in contrast to the 2D synthetic jet case. Of course such conclusions should be considered with care, because two different types of actuation are considered. However, from the results in this work it is clear that 3D effects should be taken into account to obtain the most efficient device for separation control.

Future work includes the simulation of a series of synthetic jet actuators, i.e. the 3D unsteady case, in order to study the mixing mechanism for this type of actuator as well. Furthermore, the separation control should be applied to the flap of the DLR-F15 configuration, which is more challenging due to the multi-element airfoil configuration. For the optimization algorithm more parameters should be included, such as jet velocity and chordwise location of the actuator, in order to obtain even more optimal solutions in terms of energy required for the actuation. An interesting option would be the use of overset grids to allow for an automated grid generation for more complicated geometries.

Acknowledgement

This work has been carried out in the framework of the Smart Fixed Wing Aircraft work package of the EU CleanSky program and the financial support of the EU is acknowledged.

References

[1] J. Wild, G. Wichmann, F. Haucke, I. Peltzer, and P. Scholz. Large scale separation flow control experiments within the german flow control network. *AIAA paper* 09–530.

[2] E. van der Weide, G. Kalitzin, J. Schlüter, and J. Alonso. Unsteady turbomachinery computations using massively parallel platforms. *AIAA paper* 06–421.

[3] H. Tang, S. Zhong, M. Jabbal, L. Garcillan, F. Guo, N. Wood, and C. Warsop. Towards the design of synthetic-jet actuators for full-scale flight conditions: Part 2: Low-dimensional performance prediction models and actuator design method. *Flow Turbulence Combust*, 78:309 – 329, 2007.

[4] A. Seifert and L.G. Pack. Oscillatory control of separation at high reynolds numbers. *AIAA Journal*, 37(9):1062 – 1071, September 1999.

[5] P.R. Spalart and S.R. Allmaras. One-equation turbulence model for aerodynamic flows. *Recherche aerospatiale*, 1:5–21, 1994.

[6] A. Jameson. Time dependent calculations using multigrid, with applications to unsteady flows past airfoils and wings. *AIAA paper* 91-1596.

[7] E. Smid, H. van Noort, A. Hirschberg, E. van Emden, H. de Vries, H. Stobbe, G.G.M. Zwart, and H.W.M. Hoeijmakers. Experimental study on fluidic control of a diffuser: influence of the slit geometry. *AIAA paper* 09–742, 2009.

[8] P.E. Gill, W. Murray, and M.A. Saunders. Snopt: an sqp algorithm for large-scale constrained optimization. *SIAM Review*, 47:99–131, 2005.

Copyright Statement